Türkiye Jeoloji Bülteni
Geological Bulletin of Turkey
60 (2017) 223–241
http://tjb.jmo.org.tr

3D Multi-view Stereo Modelling of an Open Mine Pit Using a Lightweight UAV

Hafif bir İHA ile bir Açık Maden Ocağının 3B Çok-bakılı Stereo Modellemesi

İnan Ulusoy*, Erdal Şen, Alaettin Tuncer, Harun Sönmez, Hasan Bayhan

Hacettepe University, Dept. of Geological Engineering, 06800, Beytepe-Ankara, Turkey

Geliş/Received : 06.09.2016 • Düzeltilmiş Metin Geliş/Revised Manuscript Received : 09.03.2017 • Kabul/Accepted : 14.03.2017 • Baskı/Printed : 01.04.2017
Araştırma Makalesi/Research Article *Türkiye Jeol. Bül. / Geol. Bull. Turkey*

Abstract: Digital elevation models have been evolved in decades, their resolution and accuracy have improved vividly. Geological, structural and geomorphological benefits of those high-quality digital elevation models enhanced the quality of the research and engineering and unfold the visibility of the data. Modern techniques such as laser scanners provide a quantum leap on digital modelling, however the cost of those methods limits their widespread usage. Improvements in stereo-photogrammetry did not decelerate. On the contrary, the evolution of Structure from Motion–Multi-view stereo-photogrammetry (SfM-MVS) method is accelerated by the continuous developments in digital photography and computer vision technologies. We have used a lightweight drone to acquire digital aerial photographs of an open mine pit for an ultimate purpose of modelling the terrain using SfM-MVS procedure. We have been able to derive a high resolution (0.3 m/pixel) DEM and a very high resolution (0.04 m/pixel) orthorectified aerial image. Both datasets are representing the topography with high sample point densities. Elevation model dataset has been compared with the regular topographic point measurements of the mine pit and the accuracy of the aerially derived model have been investigated. Sources of modelling errors, the effect of temporal physical changes in the terrain, effect and importance of geo-referencing have been discussed in detail. SfM-MVS is a cost-effective, rapid and promising technique for digital mapping, modelling and monitoring in various spatial scales of Geology.
Key Words: 3D modelling, Aerial imaging, DEM, Drone, High-resolution, Open pit mine,

Öz: *Sayısal yükseklik modelleri (SYM) on yıllar içinde evrilmiş, hassasiyetleri ve çözünürlükleri de görünür ölçüde artmıştır. Bu yüksek kaliteli SYM'lerinin jeolojik, yapısal ve jeomorfolojik faydaları bilimsel araştırmanın ve mühendislik uygulamalarının kalitesini ciddi oranda artırmış ve verinin görünürlüğünü yükseltmiştir. Lazer tarama gibi modern tekniklerin sayısal modellemede bir kuantum sıçraması yaratmasına rağmen bu metotların yüksek maliyeti uygulamalarını kısıtlamaktadır. Stereo-fotogrametrideki ilerleme ise yavaşlamamıştır. Tersine, "Hareketten Yapı–Çok bakılı stereofotogrametri" (HY-ÇBS) metodunun gelişimi sayısal fotoğraflama ve bilgisayar teknolojisindeki sürekli gelişmeyle birlikte ivmelenmiştir. Bu çalışmada, HY-ÇBS yöntemi kullanarak yeryüzü modelleme nihai amacı ile hafif bir dron kullanarak bir açık maden ocağının hava fotoğrafları alınmıştır. Yüksek çözünürlüklü (0.3 m/piksel) bir sayısal yükseklik modeli ve çok yüksek çözünürlüklü (0.04 m/piksel) bir ortorektifiye hava fotoğrafı oluşturulmuştur. Hem oluşturulan SYM, hem de hava fotoğrafı topoğrafyayı ve maden ocağını yüksek nokta yoğunluğu ile temsil etmektedir. Oluşturulan yükseklik modeli, maden ocağının olağan topoğrafik nokta ölçümleri ile kıyaslanmış ve havadan oluşturulan modelin hassasiyeti incelenmiştir. Modelleme hatalarının kaynakları, yerdeki zamanla değişen fiziksel değişikliklerin etkisi ve jeoreferanslamanın önemi detaylıca tartışılmıştır. HY-ÇBS yöntemi, sayısal haritalama ve çok çeşitli jeolojik ölçeklerde modelleme ve gözlem amacı ile kullanılabilecek, çok uygun maliyetli, hızlı ve gelecek vadeden bir tekniktir.*
Anahtar Kelimeler: *3B modelleme, Açık maden ocağı, Dron, Havadan görüntüleme, SYM, Yüksek-çözünürlük,*

**Yazışma / Correspondence: inan@hacettepe.edu.tr*

INTRODUCTION

Recent significant strides in 3D model reconstruction using Structure from Motion Multi-View Stereo-photogrammetry (SfM-MVS) algorithms in computer vision (Gong and Wang, 2011; Calakli et al. 2012) is rapidly spreading on morphology based research in various scales. Production of 3D point cloud data are no longer limited to expensive and specialised devices like laser/radar range scanners, but also possible with uncalibrated consumer market digital cameras (Furukawa and Ponce, 2007; Gong and Wang, 2011; James and Robson, 2012; Bemis et al. 2014). SfM-MVS modelling is opening a new era in earth sciences allowing widespread use of timesaving, high-resolution and multi-scale surface modelling with low cost.

Several freely available and commercial codes/software packages are available for SfM-MVS procedure (Bemis et al. 2014); upon them, a commercial software, Agisoft PhotoScan was used in this study. SfM-MVS procedure builds a simple point cloud data (Fig. 1a) using multiple images acquired from different angles, distances and positions. it builds a dense point cloud (Fig. 1b) by reanalysing this point cloud data and finally extracts surfaces and meshes from the dense point cloud (Fig. 1c, 1d). Final surfaces covering the mesh could be coloured by the pixel values in the photographs or could directly be texturized using the pieces of the photographs (Fig. 1e, 1f). Structure from Motion (SfM) theorem stands on the assumption that the structure of four non-coplanar points is recoverable from three orthographic projections (Ullman, 1979). The first stage of the 3D modelling procedure SfM uses multiple images of a scene taken from different positions, decomposes them into elements (which denote identifiable feature points such as isolated points, terminations of line segments, or texture elements) and recover their three-dimensional structure and motion (Ullman, 1979). PhotoScan uses an algorithm similar to Scale Invariant Feature Transform (SIFT - Lowe, 2004) for feature detection and generates a descriptor for each point based on its local neighbourhood (‘Agisoft’, 2016). For relatively clean, regular and dense point clouds, many existing algorithms have been developed to extract the geometric surface precisely (Gong and Wang, 2011).

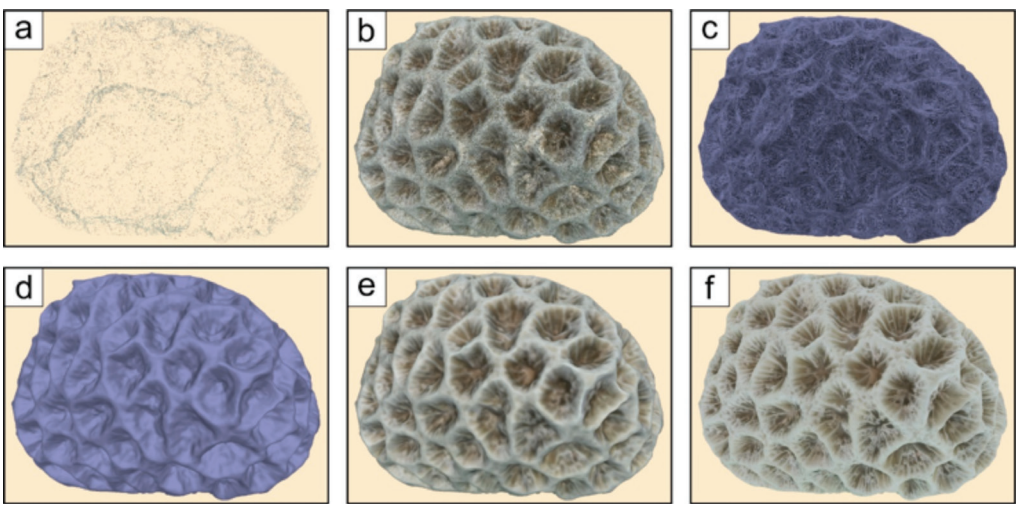

Figure 1. *Multi-View stereo model of a coral specimen a) simple point cloud, b) dense point cloud, c) mesh model, d) shaded surface model, e) colored surface model, f) texturized surface model.*

Şekil 1. *Bir mercan el örneğinin çok-bakılı stereo modeli* ***a)*** *basit nokta bulutu,* ***b)*** *yoğun nokta bulutu,* ***c)*** *kafes modeli,* ***d)*** *gölgeli yüzey modeli,* ***e)*** *renkli yüzey modeli,* ***f)*** *doku bindirilmiş yüzey modeli.*

Using matched features and camera parameters embedded in the EXIF information, a mathematical 'camera model' (along with information on camera position and orientation, if available) is built and is used to determine 3D point coordinates from the two-dimensional (2D) image coordinates (James and Robson, 2014). These values are then simultaneously optimized in a 'bundle adjustment' (Granshaw, 1980), which produces a self-consistent 3D model with associated camera parameters, by minimizing the overall residual error (James and Robson, 2014). Linking SfM output with multi-view stereo-photogrammetry (MVS) algorithms efficiently filters out noisy data and significantly increases the number of reconstructed points resulting with a high-quality data sufficient to build a surface (James and Robson, 2012).

Several interesting and useful examples from different research areas (some among many examples are Gimenez et al. 2009; Niethammer et al. 2010; James and Varley, 2012; Skarlatos and Kiparissi, 2012; Calakli et al. 2012; Tuffen et al. 2013; Bemis et al. 2014; Forte, 2014; Bennet, 2015; Burns et al. 2015; Haukaas, 2015; Shahbazi et al. 2015; Van Damme, 2015; Vepakomma et al. 2015; Tonkin et al. 2016) are shaping, contributing and defining the limitations of the new modelling technique. James and Robson (2012) demonstrated the application of SfM-MVS modelling from decimeter to kilometer scale and presented a thorough discussion on the precision of the method. Gomez and Purdie (2014) used unregistered photographs acquired by an unmanned aerial vehicle (UAV) to retrieve high-resolution 3D model of a glacier terminus and surrounding sub-vertical valley wall morphology. Tong et al. (2015) processed and integrated point cloud data generated by terrestrial laser scanning with UAV imagery and created a 3D model for mapping and monitoring of open-pit mine areas and achieved decimeter-level accuracy. Using SfM-MVS, Brothelonde et al. (2015) modelled the Yenkahe resurgent dome (Vanuatu), produced high-resolution DEM-orthophoto pair and compared the results with satellite derived DEMs. Lewis et al. (2015) created a DEM of Mammoth Mountain fumarole area, then orthorectified and georeferenced pre-dawn thermal infrared imagery onto the SfM-MVS model.

Traditional techniques such as global positioning systems (GPS) and electronic total station (TS) provide point-based observations of open-pit mine areas (Tong et al. 2015). Remote locations, mountainous surroundings and sizes of those pits often complicate the modelling and monitoring studies; the cost of these ground monitoring techniques is also rather high (Tong et al. 2015). Lightweight UAVs may provide an alternate and/or substitute data for 3D modelling and monitoring of open-pit mines.

We have used SfM-MVS method for high-resolution topographical modelling of an open-pit mine using the digital images we have acquired by a lightweight drone. Espey open mine pit is one of the largest borate mines in the world. The mine is located in the Emet basin (Kütahya, Turkey), in a close proximity to a bigger open-mine borate pit named Hisarcık. Both mines are mining for Colemanite, concentrating the mineral and mainly producing concentrated borate, boric acid and Etiboron-ceramic as final products. Since 2014, concentrated borate and boric acid production capacity of the two mines are 900,000 and 290,000 tonnes/year, respectively ('Etimaden', 2016). In the Neogene Emet basin, the borates are interlayered with tuff, claystone, and marl with limestone occurring above and below the borate lenses (Helvacı, 2015). In the Espey mine pit, borates (Figure 2a, greenish grey coloured base level) are overlain by reddish and then yellow-beige limestone-marl-claystone alternations (Figure 2a).

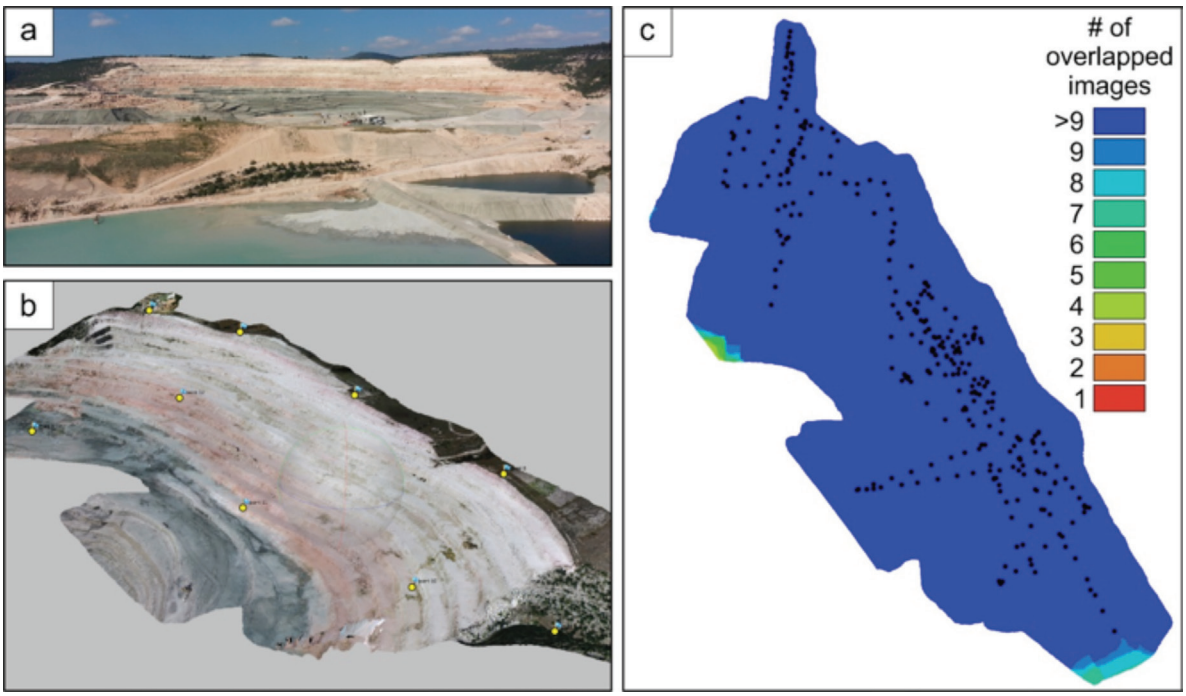

Figure 2. *Espey open-pit mine, a) photograph of the mine pit, b) 3D colored surface model of the mine pit, c) Figure showing the aerial image locations and number of overlapped images.*
Şekil 2.*Espey açık maden ocağı,* ***a)*** *ocağın fotoğrafı,* ***b)*** *ocağın 3B renkli yüzey modeli,* ***c)*** *hava fotoğraflarının lokasyonlarını ve binili görüntü sayısını gösterir şekil.*

METHODOLOGY

Topographic measurements of the open mines are regularly performed using Total Station (TS). The derived aerial model was compared with the latest TS measurement of the Espey mine. Topographic TS measurements of the area covered by the aerial model contain 4496 measurement points which was acquired by a Leica Nova TM50 monitoring station by readings at natural surface (with 2 mm ± 2 ppm accuracy). TS measurements yield a point density of 0.008 points/m^2 and a DEM resolution of 4.24 m/pixel.

UAV Imaging

We used Phantom 2 vision+ which is a lightweight (1242 g) UAV designed for image acquisition (Figure 3). The vehicle was equipped with an integrated 14 MP camera (with a wide-angle lens) mounted on a 3 axis gimbal. The focal depth of the camera is 5 mm. Images in 4384 × 3288 pixel resolution were taken every 4 seconds during the flights and recorded on 4 GB micro SD card on the vehicle. All of the images were acquired during two flights; each flight lasting approximately 16 minutes. Flights were performed by manual controlling at three different heights 80, 100 and 120 meters. The footprint of a single image is ~244 × 180 meters and the ground pixel size is ~55 mm. This allowed an approximate image overlap of 77% for image pairs (Figure 2c). Images were taken both by nadir looking angle and incidence angle approximating 45°.

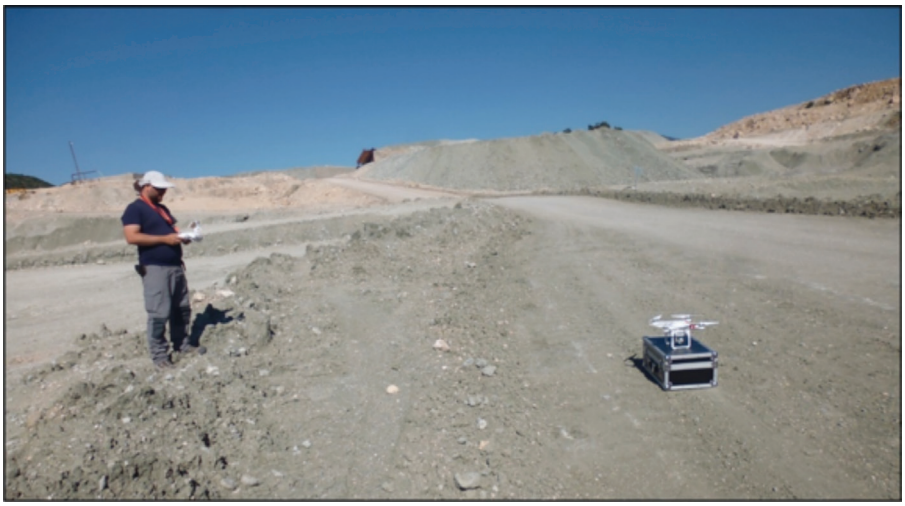

Figure 3. *Lightweight drone used to create the surface model and orthorectified image of the mine pit.*
Şekil 3. *Maden ocağının ortorektifiye görüntüsünü ve yüzey modelini yaratmak için kullanılan hafif dron.*

Aerial Topographic Modelling

491 images were acquired during the flights, 132 of them were manually eliminated as they were blurry, unfocused or accidentally shot the landing gear of the UAV. A total of 359 images were used to construct the 3D model of the mine pit (Figure 2c). The computer used for modelling was a standard notebook computer with 8 GB RAM.

3D modelling was carried out using a commercial software Agisoft Photoscan version 1.1.6 © ('Agisoft', 2016) which performs a Structure from Motion with Multi-view stereo-photogrammetric approach for reconstruction. Photo alignment was carried out using 25,306 tie points resulting with a low-density point cloud model. In the second step, the aligned photographs were used to reconstruct the high-density SfM-MVS 3D model that was comprised of 7,152,017 points. Then the mesh and the textured mesh were created from this model. High-resolution DEM and orthorectified image were the derivatives of this model. The modelling process lasted approximately 6 hours.

Nine of the TS points recorded during the topographic modelling survey were used as ground control points to geo-reference the model (Figure 2b: yellow points). RMS error of the georeferencing was calculated as 0.89 m in X-direction, 1.71 m in Y-direction and 3.9 m in Z-direction; overall RMS error of the georeferencing was calculated to be 4.3 meters. Consequences of this high referencing error was further discussed under the discussion topic.

3D MODEL OF THE MINE

The resulting model covers an area of 0.55 km^2 with long axes approaching 1.4 km vs 0.5 km; it provides a very high-resolution orthorectified image and a digital elevation model. The resolution of the orthorectified image is 0.037 m/pixel (Figure 4) while the resolution of the DEM is 0.299 m/pixel (Figure 5a) with a point density of 716.86 and 11.20 points per square meter respectively.

Figure 4 shows the high-resolution orthorectified aerial image of the borax mine; Figure 4b and Figure 4c zoom smaller areas marked with the yellow frame in the larger images (Figures 4a and 4b). Aerial image (Figure 4) is very satisfying for a wide range of geological applications.

Produced high resolution aerial imagery has a potential for use in detailed geological mapping (Figure 4a), structural analysis (Figure 4b) and in even more detailed geological, structural and geomorphological (Figure 4c) studies as an accessory dataset. Production of orthorectified aerial imagery using lightweight UAVs is a cost effective and fast response procedure which may aid periodical open mine monitoring in a four-dimensional space. In the case of monitoring pits, UAV imagery provides successful data for detailed geological mapping, helps early detection of joint/crack initiation and helps to locate weak zones such as alteration or water escape zones (eg. Yücel and Turan, 2016; Mackenzie et al. 2016; McLeod et al. 2013).

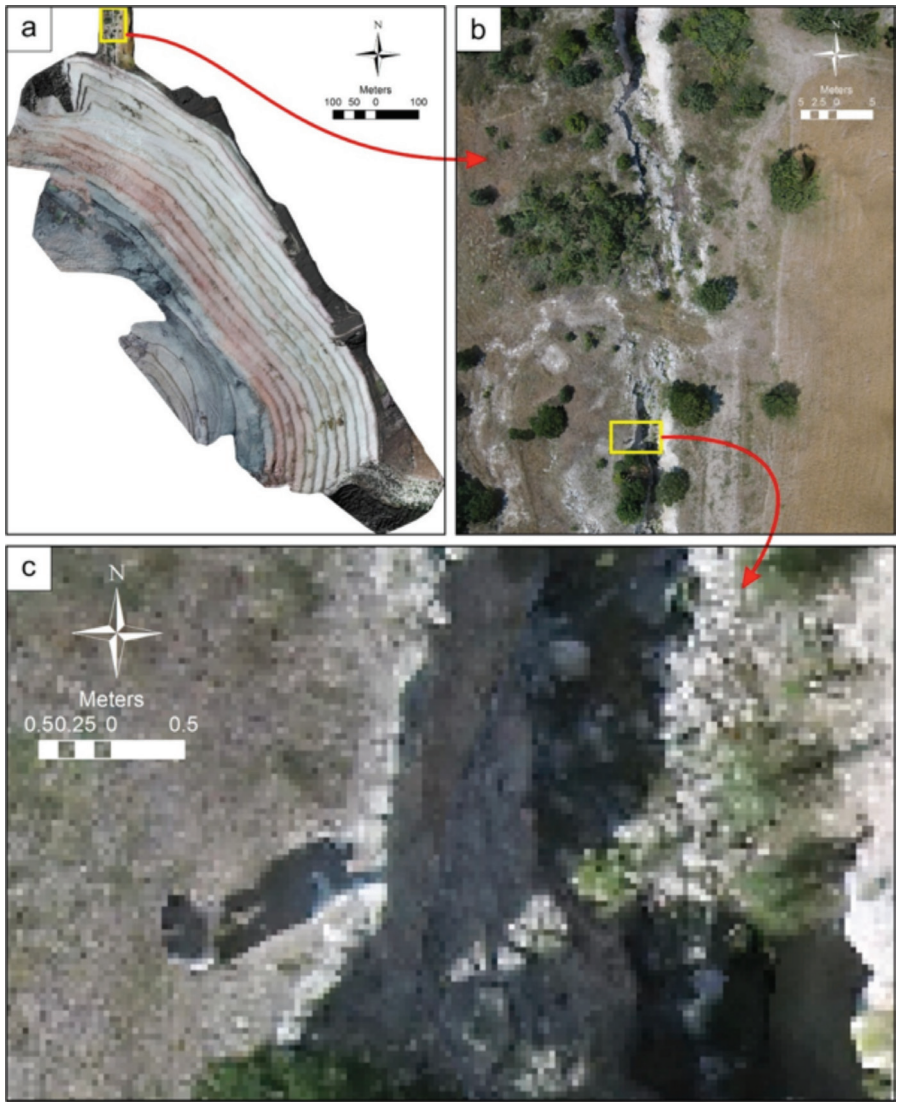

Figure 4. *Derived orthorectified aerial photograph of the a) study area, b) zoomed section of the previous photograph showing the structural detail, c) higher zoom showing the limits of the study, please note the shadow of our colleague waving the drone.*

Şekil 4. *Üretilen ortorektifiye hava fotoğrafı* ***a)*** *çalışma alanının fotoğrafı,* ***b)*** *önceki fotoğrafın yapısal detayı gösteren yakınlaştırılmış kesimi,* ***c)*** *çalışmanın sınırlarını gösteren daha yüksek yakınlaştırma, detay için dron'a el sallayan meslektaşımızın gölgesine dikkat ediniz.*

DEM derived by SfM-MVS modelling is presented in Figure 5a to provide a visual comparison with the DEM obtained by TS measurements (Figure 5b). In Figure 5, both DEMs have been presented with a colour spectrum that draped over the shaded relief products in two different sun azimuth angles (135 and 315 degrees respectively). High point density (11.20 points/m^2) of the DEM by SfM-MVS (Figure 5a) resulted in a superior DEM quality and higher resolution when compared to DEM by TS (Figure 5b). Due to lower point density (0.008 points/m^2), a false micro-hummocky terrain have been observed in DEM by TS. Sharp topographic features and bench geometry are better modelled by the SfM-MVS derived DEM (Figure 5a).

The difference between the two DEMs was further investigated both by arithmetic difference and by the percentage difference between the models (Figure 6). The arithmetic difference has been calculated by D_2-D_1 and the percentage difference have been calculated by the following formula: $[(D_1 - D_2) / ((D_1 + D_2) / 2)] \times 100$; where D_1 is the SfM-MSV derived DEM and D_2 is the TS derived DEM. Difference frequency diagram have been presented in Figure 7a. Root mean square (RMS) error on the control for the SfM-MVS model have been calculated 3.61 m and the percentage difference have been expressed within ±1.2% (Figure 6a,b). RMS error is an indicator of precision of the SfM-MVS cloud data with respect to the control (TS) data, and it has been calculated below 2 meters for the 80% and below 1 meter for the 50% of the dataset (Figure 7). Finally, we carried out a statistical comparison between two dataset. Based on the hypothesis that two dataset have no meaningful difference, t-test concerning 'paired two samples for means' results with a t-value of 1.15 (Table 1). When compared with the t-critical (1.15 < 1.96), the hypothesis is accepted stating that the difference between the two DEM sets is not meaningful and important. The margin of error in our determination is lower than 5 %.

Differences between the DEMs have been categorized into four main groups and indicated in Figure 6a: A) differences due to modelling, B) differences due to temporal physical changes, C) differences observed at bench crests and along slopes, D) nail shaped alternating differences near bench toes.

Table 1. *Results of t-test comparing two elevation models at 95% confidence level.*
Çizelge 1.*%95 güven aralığında iki yükseklik modelini kıyaslayan t-testi sonuçları.*

	TS	*Drone*
Mean	948.4461	947.4026
Variance	1797.047	1889.738
Observations	4497	4497
Pearson Correlation	0.996205	
Hyp. Mean Diff.	0	
df	1	
t Stat	1.15	
t Critical two-tail	1.96	

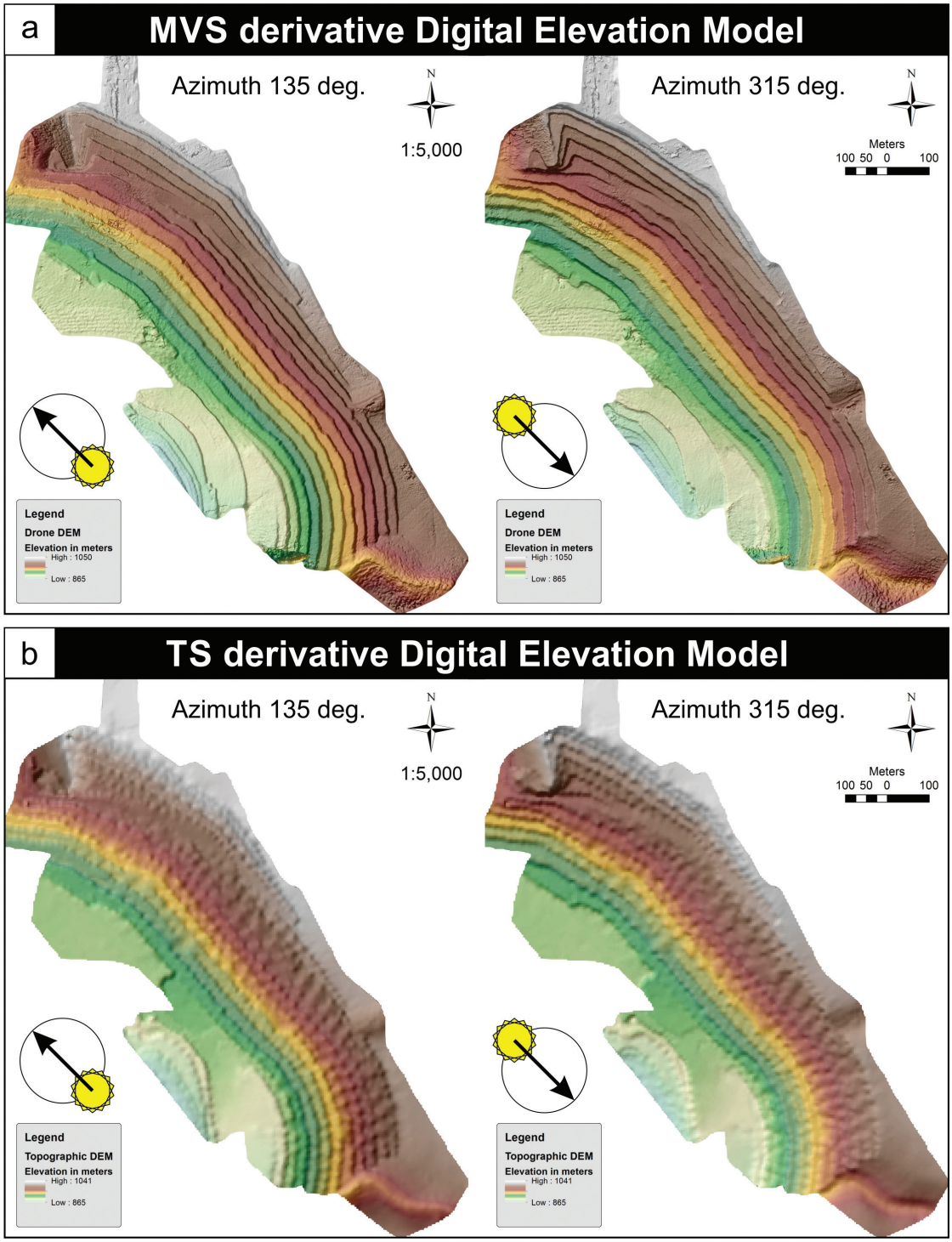

Figure 5. *Comparison of the Digital Elevation models derived by a) SfM-MVS method and by b) TS measurements under different lighting. Both DEMs are draped over a shaded relief derived from its own.*

Şekil 5. *Üretilen sayısal yükseklik modellerinin farklı ışık koşulları altında karşılaştırılması* ***a)*** *HY-ÇBS yöntemi ile oluşturulan model,* ***b)*** *TS ölçümleri ile oluşturulan model. Her iki SYM de kendilerinden türetilen gölgeli yükselti modeli üzerine oturtulmuştur.*

DISCUSSION

It is worthwhile to discuss the possible causes of differences between DEMs generated by MSV modelling and TS measurements. A common definition for precision depending on the measurement distance has been introduced by James and Robson (2012) where the relative precision rate is expressed as 'measurement precision: observation distance' (i.e. a precision of 1 centimeter over measurement distance of 10 meters is expressed as 1:1000). On various scales (from hand specimen to aerial imagery photographed by DSLR cameras) James and Robson (2012) achieved a precision rate exceeding 1:1000. Assuming the flight height of 25 meters as the measurement distance (to model a building using DSLR cameras), Esposito et al. (2014) have measured a precision rate of 1:250 on the entire model and achieved better precision than 1:500 locally. Using the lightweight UAV and 5 mm fixed focal length camera in our case, we have achieved a precision rate exceeding 3:100 for the entire model and 1:100 locally (Figure 7).

Sources of Modelling Errors

Susceptibility of the modelling depends on the variables and errors due to image acquisition, modelling method, and geo-referencing (eg. Fan et al. 2015).

Three main factors favouring a better model quality are high image resolution, an even and strong light condition and a stable image acquisition system. High image resolution can easily be achieved by digital non-metric cameras. As expected, height of the UAV during image acquisition and the resolution capability of the camera of are determinant factors for image resolution by changing the ground pixel size. On the other hand, higher image resolution requires a stronger CPU to process the increasing amount of data. Light condition drastically changes the quality of the resulting model. Our experiences showed that a decimeter scale sample requires ~80 images to build a high-quality model using artificial lighting conditions in the laboratory, while similar sample could be modelled with the same quality in the field conditions under sunlight with ~30 images. Stability of the camera during image acquisition increases the sharpness, thus the detail of the resulting model. During flight, the stability of the camera could easily be achieved using three-axis electronic gimbals.

Separate image sets acquired at different flight (thus different image acquisition) altitudes or a discontinuous image set with a gap in between may result in relatively separated or en-echelon 3D models. To exemplify this phenomenon, we have eliminated a set of images from the open mine model intensively to produce a discontinuous image set. SfM-MVS modelling of this discontinuous image set has resulted with an en-echelon model (Figure 8).

Occasions have been noted where models derived from vertical imagery show systematic broad-scale deformations, expressed as a doming (Rosnell and Honkavaara, 2012; James and Robson, 2014; Javernick et al. 2014) or concavity (Skarlatos and Kiparissi, 2012) of the central domain of the model. The doming effect results from near-parallel imaging directions (flight routes) and inaccurate correction of radial lens distortion (James and Robson, 2014). James and Robson (2014) showed that it is possible to overcome the doming effect by a collection of additional oblique images within the near-parallel imaging sets. Although we did not have additional high-resolution digital elevation data to prove analytically, we had terrain models free of doming effect just by using near-parallel image sets as well. Image sets with high overlap rates acquired with wide-angle lenses may offer a secondary formula for prevention of doming effect. 50-60% overlap between adjacent images of near-parallel imaging routes provide sufficient bundle adjustment for

3D reconstruction (e.g. Krauss, 1993; James and Robson, 2012; Abdullah et al. 2013, Bemis et al. 2014). Predefined course run with autopilot instead of manual piloting facilitates systematic data collection which for sure increases the model accuracy.

Figure 6a: 'A' exemplifies the modelling errors we have observed in the open mine pit model. The error is also clearly visible in the Figure 2b near the ground control point 10, resembling a buckled paper edge. SfM algorithms have been proved to be powerful for matching disparate imagery but can produce relatively poor feature-position precision (Remondino, 2006; Barazetti et al. 2010; James and Robson, 2012). It is possible to examine and remove these mismatch errors during early stages of modelling.

Temporal Physical Changes

While correlating two DEMs, an additional source of the arithmetic difference is the temporal physical changes in topography. Those changes include rock-falls, mass movements, slope instabilities, gravitational jointing and cracking, tectonics, vegetation and man-made changes. Rather than a source of error in 3D modelling, those changes are the subject of temporal monitoring for safety and volume estimations. SfM-MVS modelling has the capacity to monitor these changes rapidly and in high quality. Figure 6a: 'B' marks the excavated areas and rockfalls occurred between the TS measurements and UAV photography. For example, excavated volume between two topographic acquisitions was calculated to be 199,666 m^3 (Figure 6a: area drawn by dashed lines).

Differences due to Geo-referencing

One of the main factors that can affect the model accuracy is the susceptibility of the geo-referencing. When analysed in detail, the arithmetic differences of two DEMs of the open mine model presented here showed negative trending topographic changes at the southeast domain while showing positive trending topographic changes at the north-western domain of the mine (Figure 6a: C). To further investigate these trends we overlapped the two DEMs (Figure 9a) and presented the arithmetic difference map in 3D (Figure 9b). The directional trending in the difference between the DEMs is better visualized in Figure 9. It is clear that the difference on the benches is negligible but main differential errors have been observed at the bench crests and along slopes (Figure 9a,b). This phenomenon was also clarified with a graph correlating both TS points and SfM-MVS point cloud data (Figure 10) which shows that these crest/slope errors may be up to ~6 meters in horizontal and ~14 meters in the vertical direction. Even a small shift in horizontal direction may result in high vertical drop when comparing two DEMs because of the high inclination of the bench slopes. We have concluded that the axial rotations during geo-referencing cause those major differential trends between two DEMs (Figure 9b). Both a counter-clockwise rotation at z-axis and a clockwise rotation at x-axis during geo-referencing may bring forth the differential error observed in the model (Figure 9b). Most of the precision error cumulated at the bench slopes is indicating the erroneous results of a poor geo-referencing. The best way to avoid geo-referencing errors is to perform a syn-flight referencing using flags that are pre-referenced accurately.

Differences due to Uneven Resolution of DEMs

Comparing two DEMs (TS DEM via SfM-MVS DEM) with different ground resolution produces an additional differential error. TS DEM has a ground resolution of 4.24 m/pixel and a point density of 0.008 points/m^2 while the SfM-MVS DEM is superior in quality with is 0.299 m/pixel ground resolution with a point density of

11.20 points/m^2. Interpolation of lower resolution TS DEM with lower point density results in higher interpolation smoothing in the generated DEM. The interpolation smoothing in the lower resolution TS DEM appears as alternating artificial hills and depressions due to the lower density of the measurement points (Figure 9a: D). In hence, when the two sets of elevation models are compared, these artificial hills and depressions are added and subtracted and erroneously creates nail shaped alternating terrain near bench toes (Figure 6a: D).

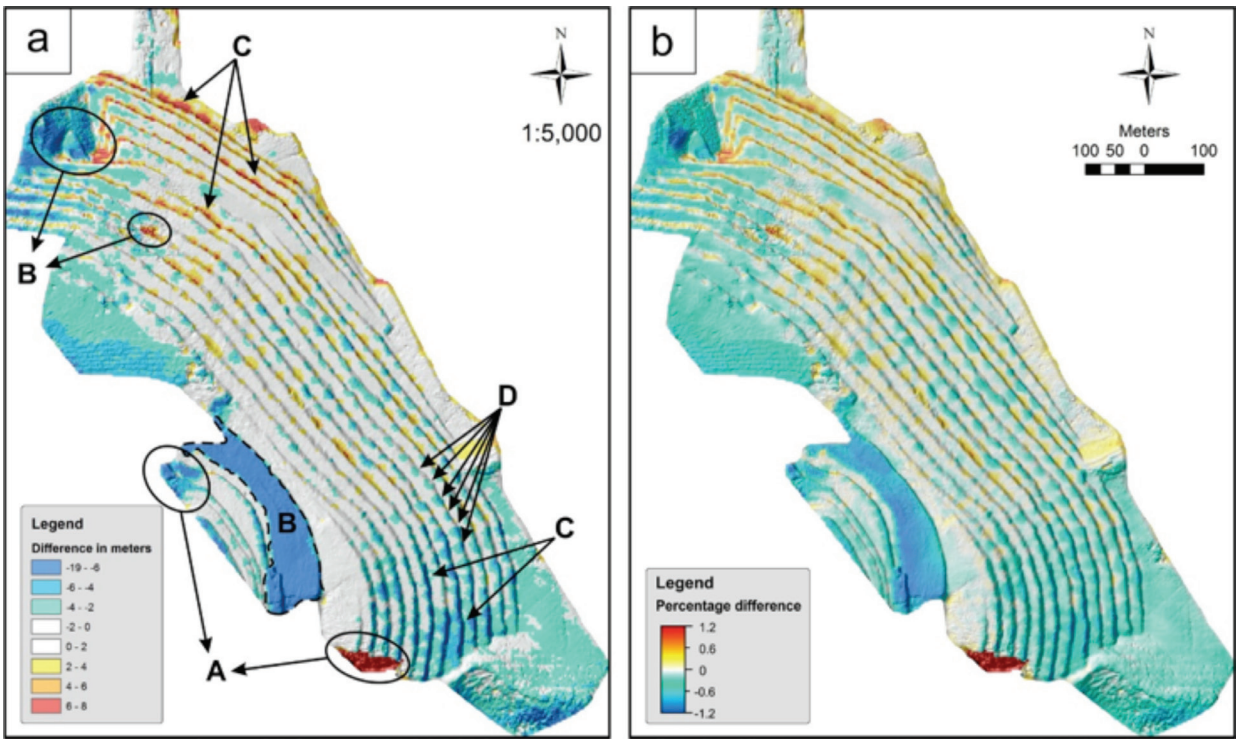

Figure 6. Arithmetic comparison of Digital elevation models, a) arithmetic difference of DEMs, b) percentage difference calculated. (A: modelling errors, B: temporal physical changes, C: differences due to geo-referencing, D: differences due to uneven resolution of DEMs, dashed line: excavated area).

Şekil 6. *Sayısal Yükseklik Modellerinin aritmetik kıyaslaması* ***a)*** *SYM'lerin aritmetik farkı ve* ***b)*** *hesaplanan yüzde farkı. (A:modelleme hataları, B: zamana bağlı fiziksel değişiklikler, C: jeo-referanslamaya bağlı farklılıklar, D: SYM'lerin farklı çözünürlükleri nedeniyle oluşan farklılıklar, kesikli çizgi: kazım alanı).*

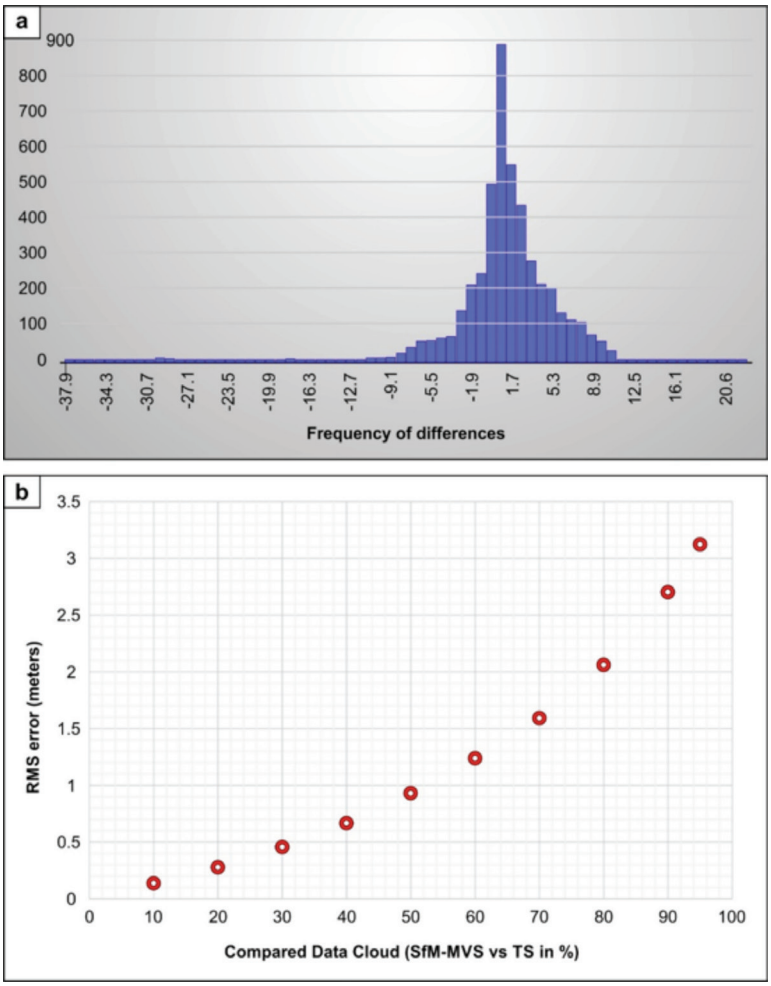

Figure 7. Accuracy of the produced model, a) Histogram of the arithmetic difference between two models, b) Graph showing the accuracy of the SfM-MVS derived elevation data with respect to TS measurements.
Şekil 7. *Oluşturulan modelin hassasiyeti, a) İki yükseklik modeli arasındaki aritmetik farkın histogramı, b) TS ölçümlerine kıyasla HY-ÇBS ile türetilmiş yükseklik verisinin hassasiyetini gösterir grafik.*

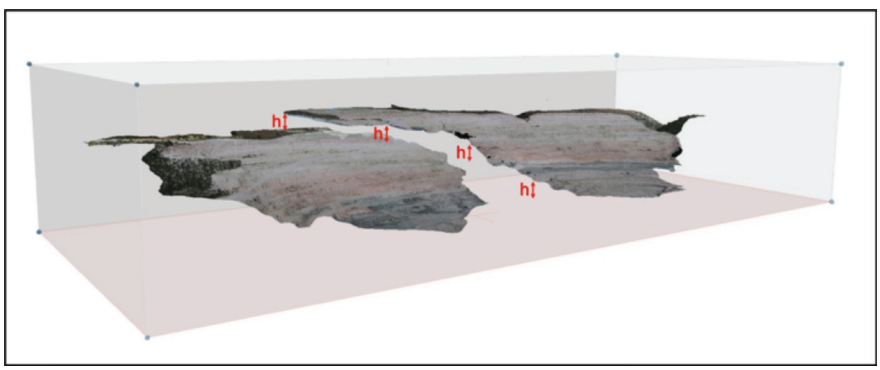

Figure 8. Erroneous en-echelon surface model generated as a result of discontinuous / incomplete image dataset.
Şekil 8. *Süreksiz / tamamlanmamış veri seti sonucu basamak şekilli hata ile oluşmuş yüzey modeli.*

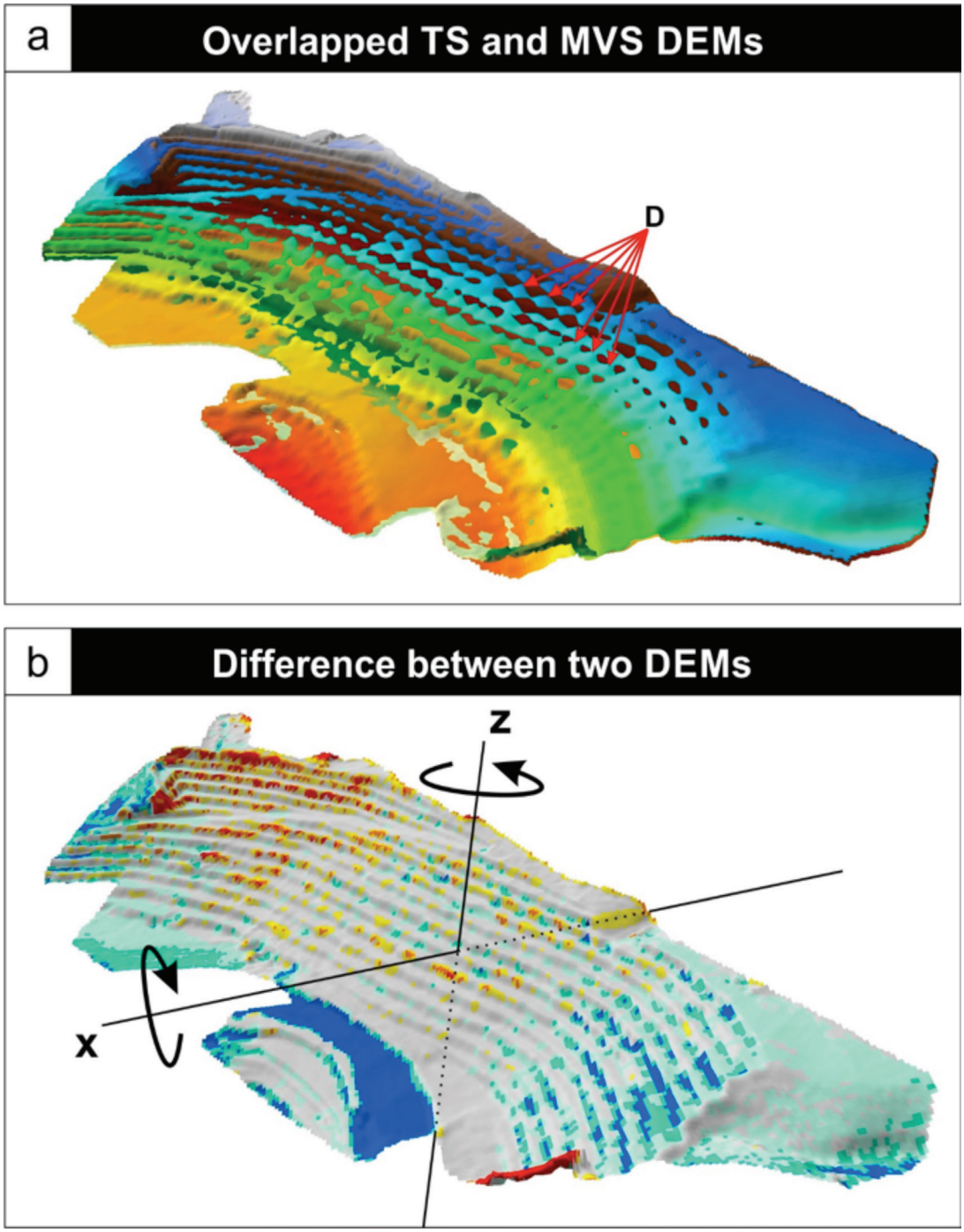

Figure 9. Visualization of the difference of two DEMs. a) Overlapped SfM-MVS and TS derived DEMs and b) 3D visualization of arithmetic difference (Figure 6a) between the DEMs.

Şekil 9. *İki SYM'nin farkının görsel olarak ifadesi. a) HY-ÇBS ve TS ile türetilen SYM'lerin üstüste çakıştırılmış hali ve b) SYM'ler arasındaki aritmetik farkın (Şekil 6a) 3B gösterimi.*

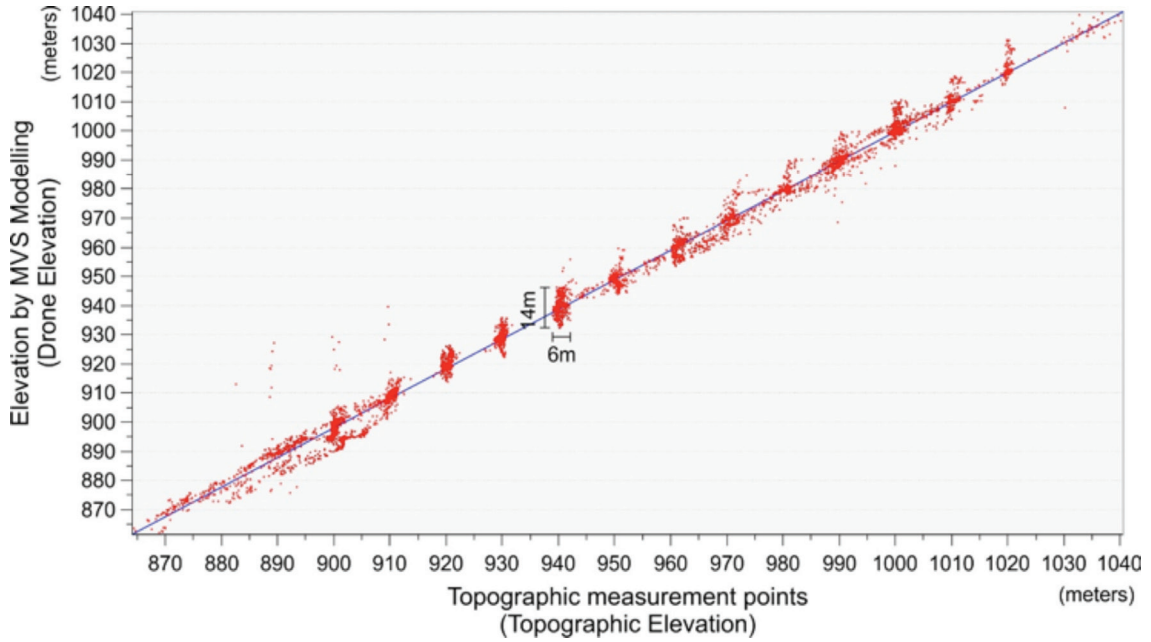

Figure 10. *Graph comparing the direct TS measurement points and coinciding elevation points derived by SfM-MVS modelling.*

Şekil 10. *TS ölçüm noktaları ve bunlara karşılık gelen HY-ÇBS modeli ile üretilmiş yükseklik değerlerini kıyaslayan grafik.*

CONCLUSION

3D modelling of open mines using lightweight UAV's and multi-view stereo modelling method is a cheap and efficient method that can fulfill the commercial and engineering needs. The method has a potential to supersede the existing expensive methods such as laser image detection and laborious methods such use mapping by point detection systems in the near future. Using low budget instrumentation and software, within a considerably short working time (including fieldwork and computer modelling) MSV with lightweight UAV provide tangible results.

Using a lightweight UAV equipped with a 5 mm fixed focal length camera which is stabilized by an electronic gimbal, we were able to produce a high resolution (0.3 m/pixel) DEM and a very high resolution (0.04 m/pixel) orthorectified aerial image. Both datasets have high point density (orthophoto: 716.86 points/m^2 and DEM: 11.20 points/m^2) and we achieved an elevation precision better than 3 m for the entire dataset and 1 m for the 50% of the dataset. Derived imagery and elevation data presents affordable, rapid and quality data for monitoring and mapping mining terranes. A discussion on the quality of the method and basic quality improvement strategies (such as syn-flight georeferencing and autonomous flight) have been explicated.

Rapid and easy execution of the modelling workflow allows temporal monitoring and helps investigating and quantifying manmade geomorphological modifications and changes due to mass movements, crack/fault formations, water and vegetation.

Future increase in flight time and payload capacity in lightweight UAVs will extend the investigation area and increase the quality of the models. Use of workstations with high RAM for modelling allows building DEMs with higher resolution. Resolution of the orthorectified imagery depends mainly on the resolution of the

camera, lighting conditions and distance from the target.

Besides geological and geomorphological applications, SfM-MVS is a promising technique for areas such as archaeology, urban planning, agriculture/forest engineering, construction engineering and preservation of cultural heritage with high precision earth modelling capabilities.

ACKNOWLEDGEMENTS

The presented work was funded by Hacettepe University Scientific Research Projects Coordination Unit with a Support project (FDS-2015-6927). The field test was supported by Eti Mine Works General Directorate, Turkey, whom we thank for permission to publish the results. The authors gratefully acknowledge the improvements by the Editor, Prof. Dr. Orhan Tatar and the anonymous Reviewer (#2).

GENİŞLETİLMİŞ ÖZET

"Hareketten yapı – Çok bakılı stereofotogrametri" (HY-ÇBS) yöntemi ile 3 Boyutlu (3B) model oluşturma çalışmalarındaki güncel atılımlar (Gong ve Wang, 2011; Calakli vd. 2012) yöntemin morfoloji kökenli çalışmalarda hızla yayılmasını sağlamıştır. 3B nokta bulutu verisinin üretilmesi artık sadece pahalı ve özelleşmiş cihazlar olan lazer / radar aralık ölçerlerle sınırlı değildir. Kalibrasyonsuz, tüketici ölçeğindeki sayısal kameralarla da 3B nokta bulutu verisi üretmek mümkündür (Furukawa ve Ponce, 2007; Gong ve Wang, 2011; James ve Robson, 2012; Bemis vd. 2014). HY-ÇBS yöntemi geniş ölçekte, çok ucuza, yüksek çözünürlüklü yüzey modellemesinin önünü açarak yerbilimlerinde yeni bir çağ açmaktadır.

HY-ÇBS yönteminde farklı açı, pozisyon ve uzaklıklardan alınan birçok görüntü yardımıyla basit bir 'nokta bulutu' oluşturulur. Bu basit nokta bulutunun tekrar işlenmesi ile bir 'yoğun nokta bulutu' ve en sonunda da bu veri setinden 'kafes-yüzey' üretilir (Şekil 1a, b, c). 'Kafes-yüzey', fotoğraflardaki piksel değerlerine göre renklendirilebilir veya yüzeyler doğrudan fotoğraftan kesilerek model üzerine yapıştırılarak bir doku oluşturulabilmektedir (Şekil 1d, e, f). 3B modelleme yönteminin ilk etabı olan Hareketten-Yapı (HY) algoritması farklı pozisyonlardan çekilmiş pek çok görüntüyü tarar, bu görüntüleri elementlerine (izole noktalar, çizgisel unsurların bitiş noktaları veya dokusal unsurlar gibi ayırdedilebilir yapısal unsurlar) ayırır ve bunların üç boyutlu yapısını ve hareketini bu unsurları tekrar birleştirerek yeniden oluşturur (Ullman, 1979). Bu ilk aşamada kullandığımız yöntem, ölçeğe göre değişmeyen unsur dönüştürme temelli bir unsur tespit algoritmasıdır (SIFT – Love, 2004) ve her nokta için noktanın lokal komşularını kullanarak bir tanım (konum, renk, doku vs.) oluşturur.

Değişik araştırma alanlarından pek çok ilgi çekici ve faydalı örnek uygulama bu yeni modelleme tekniğinin sınırlarını çizmekte, tekniğe katkıda bulunmakta ve tekniğin sınırlarını belirlemektedir (pek çok örnekten bazıları şunlardır: Gimenez vd. 2009; Niethammer vd. 2010; James ve Varley, 2012; Skarlatos ve Kiparissi, 2012; Calakli vd. 2012; Tuffen vd. 2013; Bemis vd. 2014; Bennet, 2015; Shahbazi vd. 2015; Van Damme, 2015; Vepakomma vd. 2015; Tonkin vd. 2016).

Araştırma kapsamında hafif bir dron ile alınan hava fotoğrafları kullanılarak, HY-ÇBS yöntemi ile bir açık maden ocağının yüksek çözünürlüklü modellemesi gerçekleştirilmiş; oluşturulan model, ocağın olağan noktasal topoğrafik ölçümleri ile kıyaslanmıştır.

Çalışmada havadan görüntü almak için tasarlanmış hafif (1242 g) bir insansız hava aracı olan Phantom 2 vision+ kullanılmıştır (Şekil 3). Araç, 3 eksenli bir dengeleme halkasına (gimbal) oturtulmuş 14 MP çözünürlüklü bir kamera taşımaktadır. Kameranın odak derinliği

5 mm'dir. Uçuşlar sırasında 4384 x 3288 piksel çözünürlüklü görüntüler her 4 saniyede bir çekilmiş ve araç üzerindeki 4GB hafızalı bir mikro SD karta kaydedilmiştir. Tüm görüntüler iki uçuş ile alınmıştır, her bir uçuş yaklaşık 16 dakika sürmüştür. Uçuşlar 80, 100 ve 120 metre yükseklikte manuel kontrol ile gerçekleştirilmiştir. Tek bir fotoğrafın ayakizi (gösterdiği alan) ~244 x 180 metre ve yer piksel boyutu ~55 mm'dir. Bu koşul, görüntü çiftleri arasında yaklaşık %77'lik bir binili görüntü imkânı oluşturmaktadır (Şekil 2c). Görüntüler hem nadir yönlü (aşağı yönlü) bakış hem de 45° açılı bakış ile alınmıştır. Ocağın olağan nokta ölçümleri Leica Nova 50TM Total Station (TS) ile doğal yüzeyden ölçüm ile alınmıştır, TS ölçümlerinin nokta yoğunluğu 0,008 nokta/m^2 'dir, 4,24 m Sayısal Yükseklik Modeli (SYM) çözünürlüğü elde edilmiştir.

Uçuşlar süresince 491 görüntü alınmış, bunlardan 132 tanesi daha sonra net olmadığından, odaklı olmadığından veya yanlışlıkla İHA'nın iniş takımlarını çektiği için manuel olarak elenmiştir. Maden ocağının 3B modelini oluşturmak için toplamda 359 görüntü kullanılmıştır (Şekil 2c). Veriyi modellemek için kullanılan bilgisayar 8 GB RAM'a sahip bir dizüstü bilgisayardır.

3B modelleme Hareketten-yapı ve Çok-bakılı stereofotogrametrik yöntem kullanan lisanslı Agisoft Photoscan© ('Agisoft', 2016) yazılımı (sürüm 1.1.6) ile gerçekleştirilmiştir. Fotoğraf hizalama 25.306 bağlantı noktası kullanılarak yapılmış ve düşük yoğunluklu nokta bulut modeli oluşturulmuştur. İkinci aşamada hizalanmış fotoğraflar 7.152.017 noktadan oluşan yüksek yoğunluklu 3B HY-ÇBS modelini oluşturmak için kullanılmıştır. Daha sonra kafes ve doku eklenmiş kafes bu yüksek yoğunluklu modelden oluşturulmuştur. Yüksek çözünürlüklü SYM ve ortorektifiye görüntüler bu modelden türetilmiştir. Modelleme süreci yaklaşık 6 saat sürmüştür. TS noktalarının dokuz tanesi jeoreferanslama için yer kontrol noktası olarak kullanılmıştır (Şekil 2b: sarı noktalar). Jeoreferanslama işleminin RMS hatası X-yönünde 0,89 m, Y-yönünde 1,71 m, Z-yönünde 3,9 m ve genel olarak da 4,3 metre olarak hesaplanmıştır. Bu yüksek referanslama hata payının sonuçları tartışma bölümünde irdelenmiştir.

Hafif bir İHA kullanarak, yüksek çözünürlüklü (0,299 m/piksel) bir SYM (Şekil 5a) ve çok yüksek çözünürlüklü (0,037 m/piksel) bir ortorektifiye hava fotoğrafı (Şekil 4) üretilmiştir. Her iki veri seti de yüksek nokta yoğunluğuna sahiptir (ortofoto: 716,86 nokta/m^2 ve SYM: 11,20 nokta/m^2). Oluşturulan model 0,55 km^2'lik bir alanı kaplamaktadır ve uzun eksenleri 1,4 km'ye 0,5 km uzunluğundadır. HY-ÇBS modelleme yöntemiyle türetilmiş SYM ile ocağın olağan TS ölçüm sonuçları kıyaslanmış, havadan üretilen modelin hassasiyeti sorgulanmıştır (Şekiller 6, 7, 9 ve 10). Oluşturulan modelin tamamı için 3 metreden daha hassas, veri setinin %50'si için de 1 metreden daha hassas yükseklik doğruluğu elde edilmiştir. İki veri setinin t-testi ile kıyaslanması sonucunda veri setleri arasındaki farkın anlamsız ve önemsiz olduğu gösterilmiştir (Çizelge 1). Bu yargımızda hata payı %5'in altındadır.

Modellme kaynaklı farklılıklar, zamana bağlı fiziksel değişiklikler, jeo-referanslamaya bağlı farklılıklar ve SYM'lerin aynı olmayan çözünürlüğüne bağlı farklılıklar tartışılmış, basit kalite artırma stratejileri önerilmiştir (otonom uçuş ve uçuş ile eş zamanlı jeoreferanslama gibi).

Hafif İHA'lar kullanılarak çok-bakılı stereo modelleme yöntemi ile açık maden ocaklarının 3B modellemesi ticari ve mühendislik ihtiyaçlarını karşılayabilecek ucuz ve etkili bir yöntemdir. Yöntem, yakın gelecekte lazer görüntü alımı gibi pahalı ve nokta haritalama gibi zahmetli yöntemlerin yerini alabilecek potansiyele sahiptir. Düşük bütçeli enstrümantasyon ve yazılım kullanılarak dikkate değer ölçüde kısa çalışma zamanıyla (arazi ve bilgisayar modellemesi bir arada) hafif İHA ile ÇBS güvenilir sonuçlar verebilmektedir.

Modelleme iş akışının hızlı ve kolay uygulanabilirliği zamana bağlı değişiklikleri gözlemlemeye, suni jeomorfolojik değişiklikleri, kütle hareketlerine, kırık çatlak oluşumlarına, su ve vejetasyona bağlı değişimleri incelemeye ve sayısallaştırmaya olanak sağlamaktadır.

Hafif İHA'ların uçuş zamanında ve yük kapasitelerinde yakın zamanda meydana gelecek artış, model kalitesini ve inceleme alanını artıracaktır. Yüksek hafızalı bilgisayar istasyonların kullanımı daha yüksek çözünürlüklü modeller üretmeye olanak tanımaktadır. Ortorektifiye görüntünün çözünürlüğü esas olarak kamera çözünürlüğüne, ışık koşullarına ve hedefe olan uzaklığa bağlıdır.

Jeolojik ve jeomorfolojik uygulamaların yanısıra, HY-ÇBS, yüksek hassasiyetli modelleme kapasitesiyle arkeoloji, şehir planlama, ziraat/ orman mühendisliği, yapı mühendisliği ve kültürel varlıkların korunması alanlarında gelecek vadeden bir yöntemdir.

REFERENCES

Abdullah, Q., Bethel, J., Hussain, M., Munjy, R., 2013. Photogrammetric project and mission planning. In Manual of Photogrammetry, in: McGlone, J.C. (Ed.), American Society for Photogrammetry and Remote Sensing: Bethesda. MD, pp. 1187–1220.

Agisoft [WWW Document], 2016. URL http://www.agisoft.com/ (accessed 1.30.16).

Barazzetti, L., Scaioni, M., Remondino, F., 2010. Orientation and 3D modelling from markerless terrestrial images: Combining accuracy with automation. The Photogrammetric Record 25, 356–381. doi:10.1111/j.1477-9730.2010.00599.x

Bemis, S.P., Micklethwaite, S., Turner, D., James, M.R., Akciz, S., Thiele, S.T., Bangash, H.A., 2014. Ground-based and UAV-Based photogrammetry: A multi-scale, high-resolution mapping tool for structural geology and paleoseismology. Journal of Structural Geology 69, 163–178. doi:10.1016/j.jsg.2014.10.007

Bennet, M.J., 2015. Evaluating the Creation and Preservation Challenges of Photogrammetry-based 3D Models. UConn Libraries Published Works. Paper 52.

Brothelande, E., Lénat, J.-F., Normier, A., Bacri, C., Peltier, A., Paris, R., Kelfoun, K., Merle, O., Finizola, A., Garaebiti, E., 2015. Insights into the evolution of the Yenkahe resurgent dome (Siwi caldera, Tanna Island, Vanuatu) inferred from aerial high-resolution photogrammetry. Journal of Volcanology and Geothermal Research 299, 78. doi:10.1016/j.jvolgeores.2015.04.006

Burns, J.H.R., Delparte, D., Gates, R.D., Takabayashi, M., 2015. Integrating structure-from-motion photogrammetry with geospatial software as a novel technique for quantifying 3D ecological characteristics of coral reefs. PeerJ 3:e1077. doi:10.7717/peerj.1077

Calakli, F., Ulusoy, O.A., Restrepo, M., Taubin, G., Mundy, L.J., 2012. High resolution surface reconstruction from multi-view aerial imagery [WWW Document]. Second International Conference on 3D Imaging, Modeling, Processing, Visualization and Transmission (3DIMPVT). doi:10.1109/3DIMPVT.2012.54

Esposito, S., Fallavollita, P., Wahbeh, W., Nardinocchi, C., Balsi, M., 2014. Performance evaluation of UAV photogrammetric 3D reconstruction, in: Geoscience and Remote Sensing Symposium (IGARSS). IEEE, Quebec City, QC, pp. 4788–4791. doi:10.1109/IGARSS.2014.6947565

Etimaden [WWW Document], 2016. URL http://www.etimaden.gov.tr/tr/page/uretim-emet (accessed 1.29.16).

Fan, L., Smethurst, J.A., Atkinson, P.M., Powrie, W. 2015. Error in target-based georeferencing and registration in terrestrial laser scanning. Computers and Geosciences 83, 54-64.

Forte, M., 2014. 3D ARCHAEOLOGY New Perspectives and Challenges – The Example of Çatalhöyük. Journal of Eastern Mediterranean Archaeology and Heritage Studies 2(1).

Furukawa, Y., Ponce, J., 2010. Accurate, dense, and robust multiview stereopsis. IEEE transactions on pattern analysis and machine intelligence. 8.

Gimenez, R., Marzolff, I., Campo, M., Seeger, M., Ries, J., Casali, J., Alvarez-Mozos, J., 2009. Accuracy of high-resolution photogrammetric measurements of gullies with contrasting morphology. Earth

Surface Processes and Landforms 34, 1915–1926. doi:10.1002/esp.1868

Gomez, C., Purdie, H., 2014. High-resolution monitoring of glacier and valley with combined ground- and UAV-based Photogrammetry: Study of fox valley, New Zealand, in: IEEE International Conference on Aerospace Electronics and Remote Sensing Technology (ICARES). Indonesia.

Gong, Y., Wang, Y.-F., 2011. Multi-view stereo point clouds visualization. Lecture Notes in Computer Science 281–290. doi:10.1007/978-3-642-24028-7_26

Granshaw, S.I., 1980. Bundle adjustment methods in engineering photogrammetry. The Photogrammetric Record 10, 181–207. doi:10.1111/j.1477-9730.1980.tb00020.x

Haukaas, C., 2015. New opportunities in digital archaeology: The use of low-cost Photogrammetry for 3D documentation of archaeological objects from Banks island, NWT (Electronic Thesis and Dissertation Repository No. Paper 2117.).

Helvacı, C., 2015. Geological Features of Neogene Basins Hosting Borate Deposits: An Overview of Deposits and Future Forecast, Turkey. Bulletin of The Mineral Research and Exploration 151, 169–215. doi:10.19111/bmre.05207

James, M.R., Robson, S., 2012. Straightforward reconstruction of 3D surfaces and topography with a camera: Accuracy and geoscience application. Journal of Geophysical Research 117, F03017. doi:10.1029/2011jf002289

James, M.R., Robson, S., 2014. Mitigating systematic error in topographic models derived from UAV and ground-based image networks. Earth Surface Processes and Landforms 39, 1413–1420. doi:10.1002/esp.3609

James, M.R., Varley, N., 2012. Identification of structural controls in an active lava dome with high resolution DEMs: Volcán de Colima, Mexico. Geophysical Research Letters 39, L22303. doi:10.1029/2012gl054245

Javernick, L., Brasington, J., Caruso, B., 2014. Modeling the topography of shallow braided rivers using structure from motion photogrammetry. Geomorphology 213, 166–182. doi:10.1016/j.geomorph.2014.01.006

Kraus, K., 1993. Photogrammetry, Vol. 1: Fundamentals and standard processes. Dümmlers.

Lewis, A., Hilley, G.E., Lewicki, J.L., 2015. Integrated thermal infrared imaging and structure-from-motion photogrammetry to map apparent temperature and radiant hydrothermal heat flux at mammoth mountain, CA, USA. Journal of Volcanology and Geothermal Research 303, 16–24. doi:10.1016/j.jvolgeores.2015.07.025

Lowe, D.G., 2004. Distinctive image features from scale-invariant Keypoints. International Journal of Computer Vision 60, 91–110. doi:10.1023/b:visi.0000029664.99615.94

Mackenzie, D., Elliott, J.R., Altunel, E., Walker, R.T., Kurban, Y.C., Schwenninger, J.-L., Parsons, B., 2016. Seismotectonics and rupture process of the MW 7.1 2011 Van reverse-faulting earthquake, eastern Turkey, and implications for hazard in regions of distributed shortening. Geophysical Journal International, 206 (1), 501-524.

McLeod, T., Samson, C., Labrie, M., Shehata, K., Mah, J., Lai, P., Wang, L., Elder, J.H., 2013. Using video acquired from an unmanned aerial vehicle (UAV) to measure fracture orientation in an open-PIT mine. Geomatica, 67(3), 173-180.

Niethammer, U., Rothmund, S., James, M.R., Travelletti, J., Joswig, M., 2010. UAV-Based Remote Sensing of Landslides. International Archives of Photogrammetry, Remote Sensing and Spatial Information Sciences, Commission V Symposium, Newcastle upon Tyne, UK. Vol. XXXVIII, Part 5.

Remondino, F., 2006. Detectors and descriptors for photogrammetric applications. International Archives of the Photogrammetry, Remote Sensing and Spatial Information Sciences: Symposium of ISPRS Commission III Photogrammetric Computer Vision PCV ’06, Int. Soc. for Photogramm. and Remote Sens., Bonn, Germany. 36, 49–54.

Rosnell, T., Honkavaara, E., 2012. Point cloud generation from aerial image data acquired by a Quadrocopter type micro unmanned aerial vehicle and a digital still camera. Sensors 12, 453–480. doi:10.3390/s120100453

Shahbazi, M., Sohn, G., Théau, J. and Ménard, P., 2015. UAV-based point cloud generation for open-pit mine modelling. The international archives of

the Photogrammetry, Remote Sensing and Spatial Information Sciences, vol XL-1W4, 313-320.

Skarlatos, D., Kiparissi, S., 2012. Comparison of Laser Scanning, Photogrammetry and SfM-MVS Pipeline Applied in Structures and Artificial Surfaces, in: ISPRS Annals of the Photogrammetry, Remote Sensing and Spatial Information Sciences, XXII ISPRS Congress. Melbourne, Australia.

Tong, X., Liu, X., Chen, P., Liu, S., Jin, Y., Li, L., Xie, H., Luan, K., 2015. Integration of UAV-Based Photogrammetry and terrestrial laser scanning for the Three-Dimensional mapping and monitoring of open-pit mine areas. Remote Sensing 7, 6635–6662. doi:10.3390/rs70606635

Tonkin, T.N., Midgley, N.G., Cook, S.J., Graham, D.J., 2016. Ice-cored moraine degradation mapped and quantified using an unmanned aerial vehicle: A case study from a polythermal glacier in Svalbard. Geomorphology (in press). doi:10.1016/j.geomorph.2015.12.019

Tuffen, H., James, M.R., Castro, J.M., Schipper, C.I., 2013. Exceptional mobility of an advancing rhyolitic obsidian flow at Cordón Caulle volcano in Chile. Nature Communications 4. doi:10.1038/ncomms3709

Ullman, S., 1979. The interpretation of structure from motion. Proceedings of the Royal Society of London B: Biological Sciences 203, 405–426. doi:10.1098/rspb.1979.0006

Van Damme, T., 2015. Computer Vision Photogrammetry For Underwater Archaeological Site Recording In A Low-Visibility Environment, in: The International Archives of the Photogrammetry, Remote Sensing and Spatial Information Sciences, Underwater 3D Recording and Modeling. Piano di Sorrento, Italy. doi:10.5194/isprsarchives-XL-5-W5-231-2015

Vepakomma, U., Cormier, D., Thiffault, N., 2015. Potential of Uav based Convergent Photogrammetry in monitoring regeneration standards, in: ISPRS - International Archives of the Photogrammetry, Remote Sensing and Spatial Information Sciences. Toronto, Canada, pp. 281–285. doi:10.5194/isprsarchives-XL-1-W4-281-2015

Yücel, M.A., Turan, R.Y., 2016. Areal Change Detection and 3D Modeling of Mine Lakes Using High-Resolution Unmanned Aerial Vehicle Images. Arabian Journal for Science and Engineering, 41(12), 4867-4878.